A Testing Framework for Grid-Forming Resources

Preprint

Shahil Shah,[1] Weihang Yan,[1] Przemyslaw Koralewicz,[1] Vahan Gevorgian,[1] Deepak Ramasubramanian,[2] Robb Wallen,[1] Anderson Hoke,[1] Benjamin Kroposki,[1] and Barry Mather[1]

1 National Renewable Energy Laboratory
2 Electric Power Research Institute

To be presented at the 2023 IEEE Power and Energy Society General Meeting
Orlando, Florida
July 16–20, 2023

NREL is a national laboratory of the U.S. Department of Energy
Office of Energy Efficiency & Renewable Energy
Operated by the Alliance for Sustainable Energy, LLC

This report is available at no cost from the National Renewable Energy Laboratory (NREL) at www.nrel.gov/publications.

Contract No. DE-AC36-08GO28308

Conference Paper
NREL/CP-5D00-84604
May 2023

A Testing Framework for Grid-Forming Resources

Preprint

Shahil Shah,[1] Weihang Yan,[1] Przemyslaw Koralewicz,[1] Vahan Gevorgian,[1] Deepak Ramasubramanian,[2] Robb Wallen,[1] Anderson Hoke,[1] Benjamin Kroposki,[1] and Barry Mather[1]

1 National Renewable Energy Laboratory
2 Electric Power Research Institute

Suggested Citation
Shah, Shahil, Weihang Yan, Przemyslaw Koralewicz, Vahan Gevorgian, Deepak Ramasubramanian, Robb Wallen, Anderson Hoke, Benjamin Kroposki, and Barry Mather. 2023. *A Testing Framework for Grid-Forming Resources: Preprint*. Golden, CO: National Renewable Energy Laboratory. NREL/CP-5D00-84604. https://www.nrel.gov/docs/fy23osti/84604.pdf.

NREL is a national laboratory of the U.S. Department of Energy
Office of Energy Efficiency & Renewable Energy
Operated by the Alliance for Sustainable Energy, LLC

This report is available at no cost from the National Renewable Energy Laboratory (NREL) at www.nrel.gov/publications.

Contract No. DE-AC36-08GO28308

Conference Paper
NREL/CP-5D00-84604
May 2023

National Renewable Energy Laboratory
15013 Denver West Parkway
Golden, CO 80401
303-275-3000 • www.nrel.gov

NOTICE

This work was authored in part by the National Renewable Energy Laboratory, operated by Alliance for Sustainable Energy, LLC, for the U.S. Department of Energy (DOE) under Contract No. DE-AC36-08GO28308. Funding provided by U.S. Department of Energy Office of Electricity, Office of Energy Efficiency and Renewable Energy Wind Energy Technologies Office, and under the Solar Energy Technologies Office Award Number 38637. The views expressed herein do not necessarily represent the views of the DOE or the U.S. Government.

A Testing Framework for Grid-Forming Resources

Shahil Shah[1], Weihang Yan[1], Przemyslaw Koralewicz[1], Vahan Gevorgian[1], Deepak Ramasubramanian[2], Robb Wallen[1], Anderson Hoke[1], Benjamin Kroposki[1], and Barry Mather[1]

[1]National Renewable Energy Laboratory, Golden, CO 80401, USA
[2]Electric Power Research Institute (EPRI), Knoxville, Tennessee, USA
Email: Shahil.Shah@nrel.gov

***Abstract*–This paper presents a testing framework for grid-forming (GFM) resources. First, it analytically derives in the frequency domain the active and reactive power response of an ideal voltage source with a reactor. These transfer functions are then used to quantify the voltage source behavior expected from a GFM inverter within subtransient timescales (5–15 cycles) following a grid disturbance. The paper also shows that the testing of a GFM inverter might require a reactor of an appropriate size between the inverter and the grid simulator used for the inverter testing. Finally, the paper presents a systematic approach for developing specifications for GFM resources using active and reactive power response frequency scans. The testing framework and results presented in this paper are demonstrated using EMT-PSCAD simulations of a 1-MW GFM inverter.**

I. Introduction

Historically, synchronous generators have maintained the stability of power systems by controlling the magnitude and frequency of voltages at different nodes in the electrical network. Increasing shares of inverter-based resources (IBRs) and the consequent reduction in the number of synchronous generators, however, are increasing the number of stability problems in power systems. At present, most IBRs are controlled as a current source with their current output following the grid voltage depending on the desired active and reactive power output. Although these grid-following (GFL) IBRs can contribute to voltage and frequency control, they do not provide voltage and frequency control support during shortest subtransient timescales (5–15 cycles); GFL IBRs tend to maintain constant active and reactive power output in subtransient timescales after a grid disturbance by letting the magnitude and phase of the voltages at their terminals vary during those timescales. The stable operation of power systems with high shares of IBRs (approaching 100%) requires advanced inverter controls so that the IBRs can provide voltage and frequency control in subtransient timescales. Advanced inverter controls, termed grid-forming (GFM), can achieve this by enabling IBRs to maintain constant magnitude and phase of voltages at their terminal in subtransient timescales after a grid disturbance [1].

This work was authored by the National Renewable Energy Laboratory, operated by Alliance for Sustainable Energy, LLC, for the U.S. Department of Energy (DOE) under Contract No. DE-AC36-08GO28308. Funding provided by U.S. Department of Energy Office of Electricity, Office of Energy Efficiency and Renewable Energy Wind Energy Technologies Office, and under the Solar Energy Technologies Office Award Number 38637. The views expressed in the article do not necessarily represent the views of the DOE or the U.S. Government. The U.S. Government retains and the publisher, by accepting the article for publication, acknowledges that the U.S. Government retains a nonexclusive, paid-up, irrevocable, worldwide license to publish or reproduce the published form of this work, or allow others to do so, for U.S. Government purposes.

The power system industry has identified the value of GFM controls and developed several guidelines for their core functional requirements [2]–[5]. These core functional requirements result from an expectation that a GFM inverter should behave like an ideal voltage source with physical reactance in subtransient timescales. One of the core functional requirements is that a GFM inverter should quickly dispatch active and/or reactive power within subtransient timescales following a grid disturbance depending on the characteristics of the grid at its terminal; however, it is difficult to translate the functional requirements to enforceable specifications because of the lack of clear guidance on the test setup and test procedures for GFM resources. This has forced system operators that are looking to encourage the adoption of GFM technologies to develop guidelines that are easier to meet and that might not fully use the stabilizing potential of GFM technologies. For example, the non-mandatory specifications ratified by National Grid ESO in January 2022 require GFM plants in Great Britain to start responding to different types of grid events within 5 ms; it does not define the magnitude of the full response, the maximum time taken to achieve the full response, and the duration for which the response must be sustained.

This discussion shows that it is critical to define the test setup and test procedures for quantifying the performance of GFM resources, which can then be used for developing their specifications. This paper presents a framework for testing the performance of GFM resources to address these challenges. It starts with the frequency-domain modeling of the active and reactive power response of an ideal voltage source with a reactor to provide a baseline for characterizing the internal voltage source of a GFM inverter. The paper also evaluates the impact of the test setup on the performance of GFM inverters. The paper presents a few examples on how the proposed testing framework can be used for developing specifications for GFM resources.

II. Active and Reactive Power Response of an IBR

The instantaneous active and reactive power output of an IBR are related with the d- and q-axis components of the three-phase voltages and currents at its terminal, as follows:

$$p = \frac{3}{2}(v_d i_d + v_q i_q) \text{ and } q = \frac{3}{2}(-v_d i_q + v_q i_d) \quad (1)$$

As shown in [6], the perturbations in the magnitude and phase of three-phase voltages are related with the dq components as:

$$V_m(s) = V_d(s) \text{ and } \theta(s) = V_q(s)/V_1 \quad (2)$$

where V_1 is the peak of the phase voltages at the IBR terminal.

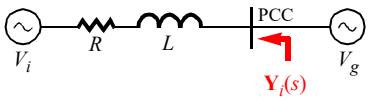

Fig. 1. Internal voltage source, V_i, with a physical reactor.

The dq components of the voltages and current at the terminal of an IBR are related as follows:

$$-\begin{bmatrix} I_d(s) \\ I_q(s) \end{bmatrix} = \begin{bmatrix} Y_{dd}(s) & Y_{dq}(s) \\ Y_{qd}(s) & Y_{qq}(s) \end{bmatrix} \begin{bmatrix} V_d(s) \\ V_q(s) \end{bmatrix} \tag{3}$$

where the second-order transfer matrix is the dq admittance of the IBR. Note that the negative sign in (3) is because of the source convention used for defining currents at the IBR terminal.

The transfer function from the magnitude and phase of the voltages to the active and reactive power output at the terminal of an IBR can be derived by linearizing (1) and using (2) and (3) as:

$$\begin{bmatrix} P(s) \\ Q(s) \end{bmatrix} = \begin{bmatrix} \frac{P_0}{V_1} - \frac{3}{2} V_1 \cdot Y_{dd}(s) & -Q_0 - \frac{3}{2} V_1^2 \cdot Y_{dq}(s) \\ \frac{Q_0}{V_1} + \frac{3}{2} V_1 \cdot Y_{qd}(s) & P_0 + \frac{3}{2} V_1^2 \cdot Y_{qq}(s) \end{bmatrix} \begin{bmatrix} V_m(s) \\ \theta(s) \end{bmatrix} \tag{4}$$

where P_0 and Q_0 represent, respectively, the steady-state active and reactive power output of the IBR.

III. Internal Voltage Source With a Reactor

In this section, we analyze the active and reactive power response of a voltage source with a physical reactor because that is how a GFM inverter is expected to behave during subtransient timescales following a grid disturbance [4]. Fig. 1 shows an internal voltage source, V_i, with a reactor (with resistance R and inductance L) connected to another ideal voltage source, V_g; the latter represents a strong grid with zero internal impedance. The dq admittance of the internal voltage source with a reactor is:

$$\mathbf{Y}_i(s) = \frac{1}{(R+sL)^2 + (\omega_1 L)^2} \begin{bmatrix} R+sL & \omega_1 L \\ -\omega_1 L & R+sL \end{bmatrix} \tag{5}$$

Using (5) in (4), the transfer function from the magnitude of the grid voltages to the reactive power output and from the phase of the grid voltages to the active power output of the internal voltage source with the reactor can be derived as follows:

$$\left.\frac{Q(s)}{V_m(s)}\right|_{\theta(s)=0} = \frac{Q_0}{V_1} - \frac{3}{2} V_1 \cdot \frac{\omega_1 L}{(R+sL)^2 + (\omega_1 L)^2} \tag{6}$$

$$\left.\frac{P(s)}{\theta(s)}\right|_{V_m(s)=0} = -Q_0 - \frac{3}{2} V_1^2 \cdot \frac{\omega_1 L}{(R+sL)^2 + (\omega_1 L)^2} \tag{7}$$

Generally, the steady-state reactive power output of IBRs is comparatively small because IBRs are not operated below a certain power factor, e.g., 0.8; hence, the first terms proportional to Q_0 on the right-hand side of (6) and (7) can be ignored. The second terms on the right hand side of (6) and (7) are equal except for a scaling factor of V_1; hence, either (6) or (7) can be used to study the active and reactive power response of an internal voltage source with a reactor.

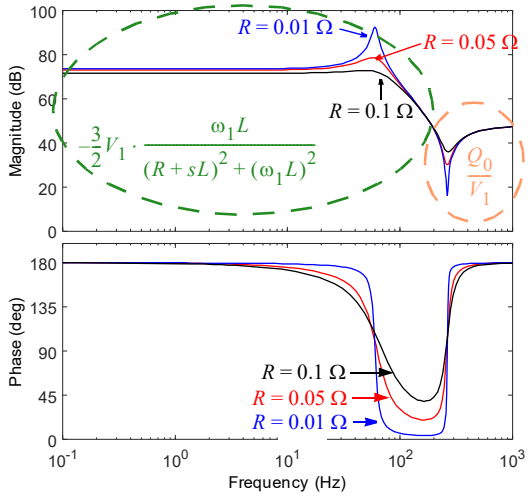

Fig. 2. Response of the transfer function from voltage magnitude to reactive power output, i.e., $Q(s)/V_m(s)$, of an internal voltage source (0.69-kV line-line rms) with a series-connected reactor with inductance, L, of 0.5 mH and resistance, R, of 0.01 Ω (blue), 0.05 Ω (red), and 0.1 Ω (black).

Fig. 2 shows the responses of the $Q(s)/V_m(s)$ transfer function obtained using (6) for different values of resistance, R, of the reactor. It is evident that $Q(s)/V_m(s)$ has a response of a second-order, low-pass filter with the corner frequency the same as the fundamental frequency of 60 Hz and the damping ratio proportional to the resistance, R. Moreover, the phase of the transfer function below the corner frequency converges to 180°. Last, for the resistance, R, that is negligible compared to the reactance, $\omega_1 \cdot L$, the steady-state gain of $Q(s)/V_m(s)$ can be approximated to $-(3/2) \cdot V_1/(\omega_1 \cdot L)$. Based on this analysis, it can be inferred that the magnitude of the reactive power response of an internal voltage source with a reactor during a voltage jump event will be inversely proportional to L, its rise time will be less than one fundamental cycle, it will be oscillatory for low values of R, and it will be in the direction opposite to the direction of the voltage jump (due to the 180° phase at low frequencies). Fig. 3 shows the reactive power response of the internal voltage source shown in Fig. 1 when the grid voltage magnitude is reduced by 10%. The frequency- and time-domain responses of an ideal voltage source with a reactor presented in this section can be used for specifying the internal voltage source of a GFM inverter.

IV. Test Setup for GFM Resources

A. PSCAD Model of a 1-MW/0.69-kV GFM Inverter

Fig. 4 shows a 1-MW/0.69-kV inverter with an LC filter that is simulated in PSCAD to explain the requirements of a test setup for GFM resources. This section shows that it is important to test a GFM inverter at an appropriate grid strength. As shown in Fig. 4, the grid impedance is assumed to be purely inductive because it is easier to test the performance of an inverter with an inductive grid

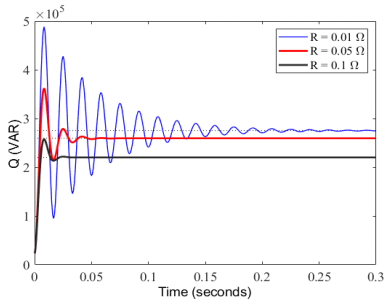

Fig. 3. Response of the reactive power output from an internal voltage source (0.69 kV line-line rms) with a reactor during a step reduction in the magnitude of the grid voltages at its terminal by 10%. Response is shown for the filter inductance, L, of 0.5 mH and resistance, R, of 0.01 Ω (blue), 0.05 Ω (red), and 0.1 Ω (black). The rise time for the reactive power output response is 5 to 15 ms, depending on the resistance of the output inductive filter of the voltage source.

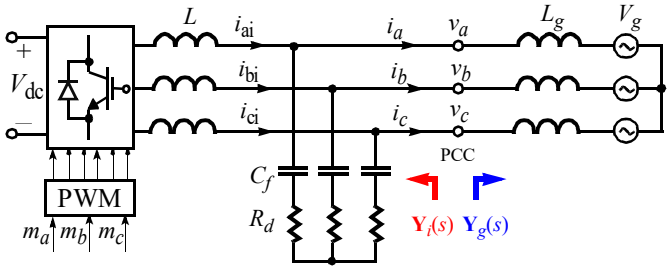

Fig. 4. Grid-connected 1-MW/0.69-kV inverter with an LC filter.

instead of a resistive grid due to the lower losses inside the reactor used for representing an inductive grid. Moreover, inductive impedance is a better representation of the grid conditions that GFM inverters would experience in the transmission network.

Fig. 5 shows the control implementation of the 1-MW GFM inverter. As shown in the figure, a voltage control loop is built on top of a current control loop. Both loops are implemented in the dq domain. The voltage magnitude reference, $v_{d,\text{ref}}$, for the voltage control loop is obtained from a slower reactive power control loop. The phase reference, θ_i, for the voltages generated by the inverter is obtained from a slower active power control loop. The circuit and control design parameters of the 1-MW inverter are not included in this paper because of the space constraint.

For all simulation results shown in this paper, P_{ref} and Q_{ref} in Fig. 5 are kept fixed, respectively, at 0.85 MW and 0.15 MVAR. Because the frequency and voltage droop control are not implemented in the active and reactive power reference shown in Fig. 5, the inverter follows the active and reactive power references in steady state even in the presence of a mismatch in the grid voltage magnitude and frequency from their nominal values.

B. Stability of a GFM Inverter for Different Grid Strengths

Because a GFM inverter is expected to behave like an ideal voltage source with a physical reactor [4], it might become unstable when it is connected to a very strong grid; hence, before testing a GFM inverter, it is important to know the range of the grid strength for which the inverter can operate in a stable manner.

Fig. 6 shows the response of the dq admittance, $\mathbf{Y}_i(s)$, of the 1-MW GFM inverter shown in Fig. 4. It is obtained using the Grid

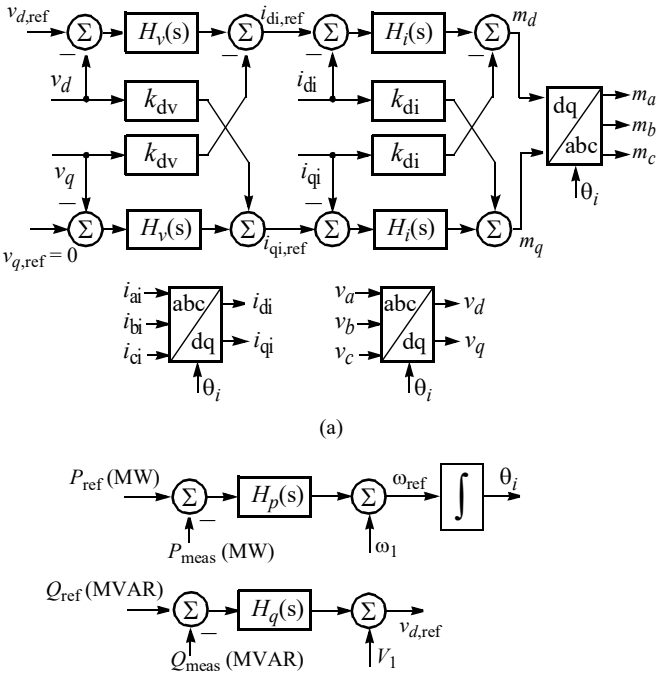

Fig. 5. Control implementation of the 1-MW/0.69-kV inverter for GFM mode: (a) inner current and voltage control loops and (b) outer active and reactive power control loops.

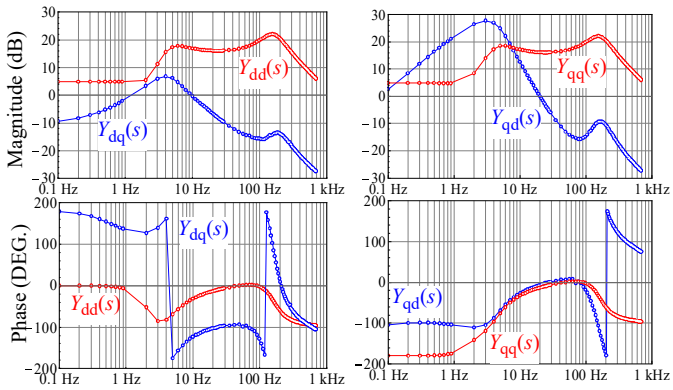

Fig. 6. DQ admittance of a 1-MW GFM inverter simulated in PSCAD obtained using NREL's Grid Impedance Scan Tool (GIST).

Impedance Scan Tool (GIST) presented in [7]. The scan of $\mathbf{Y}_i(s)$ was performed by operating the inverter with the grid inductance, L_g, of 0.5 mH, which corresponds to the grid short-circuit ratio (SCR) of 2.5. This specific value of L_g was used for the scan because the inverter was found to operate stably in the PSCAD simulations for this grid condition; note that the admittance response of the inverter obtained using the scan is independent of the grid condition. The range of grid inductance, L_g, for which the inverter can operate stably can be obtained by applying the reversed impedance-based stability criterion [8] to the loop-gain $\mathbf{Y}_i(s)\cdot\mathbf{Y}_g(s)^{-1}$, where $\mathbf{Y}_g(s)$ is the admittance of the grid, as shown in Fig. 4. The response of $\mathbf{Y}_g(s)$ for different values of L_g for the stability analysis can be obtained by using an analytical expression similar to the matrix in (5).

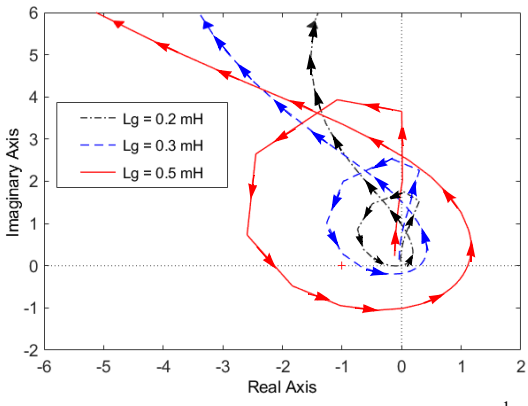

Fig. 7. Nyquist plot of the determinant of the loop gain $\mathbf{Y}_i(s)\cdot\mathbf{Y}_g(s)^{-1}$ for different grid strengths represented by grid inductance, L_g. Note that $\mathbf{Y}_g(s)$ and $\mathbf{Y}_i(s)$ are the dq admittances of the grid and the 1-MW GFM inverter, respectively.

Fig. 7 shows the Nyquist plot of the determinant of the loop gain, $\mathbf{Y}_i(s)\cdot\mathbf{Y}_g(s)^{-1}$, for different values of L_g. The number of encirclements, N, by the Nyquist plot of the critical point $(-1+j\cdot 0)$ is related with the number of unstable poles, Z, of the integrated system, i.e., the GFM inverter and the grid, and the number of unstable poles, P, of the 1-MW GFM inverter as follows [8]:

$$N = Z - P \tag{8}$$

Because the GFM inverter is stable when L_g is 0.5 mH, Z in (8) is zero for this case. Fig. 7 shows that the Nyquist plot for 0.5 mH grid inductance encircles the critical point once in the counter-clockwise (CCW) direction. The Nyquist plot would encircle the critical point twice in the CCW direction when negative frequencies are also considered; hence, N is –2 when L_g is 0.5 mH. Based on this discussion, it can be determined from (8) that P is equal to 2, i.e., the GFM inverter or $\mathbf{Y}_i(s)$ has two unstable poles. This implies that the 1-MW GFM inverter will become unstable if it is connected to an ideal voltage source, i.e., to a very strong grid. Further, because the Nyquist plots in Fig. 7 when L_g is 0.3 mH and 0.2 mH do not encircle the critical point, i.e. N is zero for these cases, it can be concluded from (8) that Z is equal to +2 for these cases. In other words, the 1-MW GFM inverter is unstable when L_g is 0.3 mH and 0.2 mH. Using this process based on the reversed impedance-based stability criterion [8], it is found that the 1-MW GFM inverter will be unstable if L_g is less than 0.35 mH, i.e., when the grid SCR is higher than 4. Moreover, the frequency of the instability predicted by the Nyquist analysis is 6.3 Hz. This analytical prediction is confirmed by the simulation results shown in Fig. 8, which shows that the 1-MW GFM inverter becomes unstable when L_g is reduced to less than 0.35 mH and it bursts into oscillations of frequency 6.3 Hz.

C. *Design of Test Setup*

This analysis shows that the admittance scan of a GFM inverter [9] can be used to determine the range of grid strengths for which the inverter can operate stably. This information can be used for selecting an appropriate size of a reactor between the inverter and the grid simulator used for the inverter testing (such as a 7-MW grid simulator facility described in [9]). This also shows that it might not be possible to test a GFM inverter directly with a grid

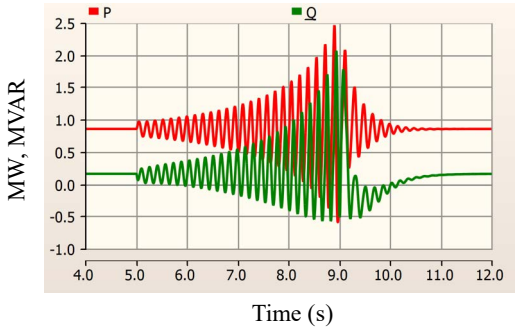

Fig. 8. Active and reactive power response of the 1-MW GFM inverter when the grid inductance is reduced at t = 5 s from 0.5 mH to 0.3 mH and increased back at t = 9 s to 0.5 mH.

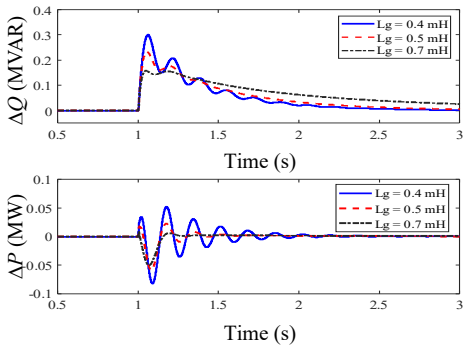

Fig. 9. Active and reactive power response of the 1-MW GFM inverter for different grid strengths, represented by grid inductance, L_g, during 10% drop in the magnitude of the infinite voltage source, V_g, in the grid.

simulator without a reactor between them if the inverter is not designed to operate stably with very strong grids. On the other hand, designing a GFM inverter to operate stably with very strong grids might require an additional reactor at the front end of the inverter, which might deteriorate the performance for other grid conditions or steady-state power transfer capability. It is important to design a GFM inverter for a wide range of grid strengths it is expected to experience during operation; however, extremely strong grid does not need be part of this range if the inverter is never going to experience such operating conditions. Note that the ability to operate with strong grids is not a design consideration for GFL inverters because they can invariably operate stably with very strong grids.

V. Testing Approach for GFM Resources

Once the reactor between a GFM inverter and the grid simulator used for experimental testing or an ideal voltage source used for simulation model-based testing is designed based on the analysis presented in the previous section†, the performance of the inverter can be tested both in the time and frequency domains. Fig. 9 shows the simulated active and reactive power response of the 1-MW inverter shown in Fig. 4 when the magnitude of the voltage source, V_g, behind the grid inductance, L_g, is reduced by 10%. The active and reactive power response are measured at the point of common coupling (PCC). As shown, the GFM inverter quickly

†. A reactor is not required between a GFM inverter and the grid simulator for inverter testing if the inverter is designed to operate stably with an ideal grid.

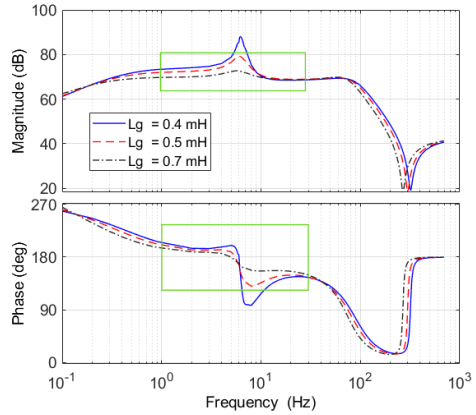

Fig. 10. Transfer function from voltage magnitude to reactive power output, i.e., $Q(s)/V_m(s)$, of the three-phase network seen from the voltage source, V_g, used for testing the 1-MW GFM inverter. The network includes the reactor with inductance, L_g, in addition to the 1-MW GFM inverter.

dispatches additional reactive power during sudden drop in the grid voltage; however, depending on the grid inductance, L_g, which is varied from 0.4 to 0.7 mH, the peak of the reactive power response is between 0.15 to 0.3 MVARs. Moreover, depending on the grid inductance, L_g, the inverter takes from approximately 30 to 60 ms for dispatching the peak reactive power response, and it is more oscillatory as the value of L_g is decreased. This behavior highlights the limitations of using only the time-domain testing of GFM inverters. Moreover, it is difficult to define specifications, such as rise time and damping, of the active/reactive power response using only the time-domain waveforms.

Fig. 10 shows the frequency scans of the transfer function from the voltage magnitude to the reactive power output of the entire network seen from the voltage source, V_g, shown in Fig. 4; hence, these frequency scans combine the effect of the reactor, L_g, with the 1-MW GFM inverter. It is not possible to evaluate such a reactive power response frequency scan independently from the active power response frequency scan if it is performed at the PCC (ref. Fig. 4) because of the coupling between them; hence, it is recommended to perform such scans at the ideal voltage source or the grid simulator used for the inverter testing. The reactive power response frequency scans in Fig. 10 exhibit almost constant magnitude approximately equal to $(3/2)\cdot V_1/(\omega_1 \cdot L)$ in the frequency range from 1 Hz to 60 Hz. Moreover, the phase response around this frequency range stays closer to 180°. Both these characteristics point to the behavior of an internal voltage source with a reactor when the scans are compared to those in Fig. 2; however, unlike the scans in Fig. 2, the frequency scans in Fig. 10 do not maintain constant magnitude and phase of 180° at frequencies less than 1 Hz. This is because droop control is not implemented in the 1-MW inverter, and hence the inverter is not expected to provide a steady-state reactive power response during a change in the grid voltage, as shown in Fig. 9. The steady state active or reactive power response is a different service and not part of the GFM controls; the GFM controls strictly focus on the ability to provide active and reactive power response in subtransient timescales; hence, we need an approximately constant magnitude response and 180° phase response in the reactive power frequency scans only at frequencies from a few hertz (1~5 Hz) to few tens of hertz (20~60 Hz) for ensuring the "internal voltage source with a reactor" behavior of the inverter in subtransient timescales. The frequency scans in Fig. 10 also show the development of a resonance near 6 Hz as the value of L_g is reduced. This matches with the stability analysis predictions in the previous section; hence, the damping of the GFM inverter in subtransient timescales can also be ensured by ensuring that the reactive power frequency scans have almost constant magnitude in the frequency range described here and a phase response close to 180° without significant variations. The green rectangles in Fig. 10 show how all these functional requirements can be "specified" using reactive power frequency scans. Similar specifications using frequency scans can also be developed for the active power response.

VI. Conclusions

This paper has presented a testing framework to evaluate core functional requirements of GFM resources that result from an expectation that a GFM resource should behave like an ideal voltage source with a reactor in subtransient timescales. The paper first modeled the frequency-domain characteristics of an ideal voltage source with a reactor and it then demonstrated how these characteristics can be used to define specifications for core functional requirements such as active and reactive power response of a GFM resource during phase and magnitude jump, respectively, in the grid voltages at the terminal. The paper also showed that a reactor might be required between a GFM inverter and a voltage source or a grid simulator used for inverter testing if the inverter is not designed to operate stably with very strong grids. Note that the proposed testing framework is not applicable for developing specifications for additional quasi steady-state functional requirements for GFM resources such as black start, primary frequency or voltage response, and harmonics.

References

[1] High Share of Inverter-Based Generation Task Force, *Grid-Forming Technology in Energy Systems Integrations.* Energy Systems Integration Group (ESIG), Reston, VA, 2022. Online: https://www.esig.energy/report-briefs.

[2] NERC (North American Reliability Corporation), *Grid Forming Technology – Bulk Power Systems Reliability Considerations.* Dec. 2021.

[3] ENTSO-E (European Network of Transmission System Operators for Electricity), *Grid-Forming Capabilities: Towards System Level Integration*. Brussels, Belgium, 2021.

[4] NGESO, GC0137: Minimum Specification Required for Provision of GB Grid Forming (GBGF) Capability, 2021.

[5] "UNIFI Specifications for Grid-forming Inverter-based Resources – Version 1," *UNIFI Consortium*, Dec. 2022.

[6] S. Shah and L. Parsa, "Impedance modeling of three-phase voltage source converters in dq, sequence, and phasor domains," *IEEE Trans. Energy Conv.*, vol. 32, no. 3, pp. 1139-1150, April 2017.

[7] S. Shah, Impedance Scan Tools for Stability Analysis of IBR Grids. G-PST/ESIG Webinar, June 2022 [Online]. Available: https://www.esig.energy/event/webinar-impedance-scan-tools-for-stability-analysis-of-ibr-grids/

[8] S. Shah, W. Yan, P. Koralewicz, E. Mendiola, and V. Gevorgian, "A reversed impedance-based stability criterion for IBR grids," in *Proc. 21st Wind Integr. Workshop*, The Hague, Netherlands, Oct. 2022.

[9] S. Shah, P. Koralewicz, V. Gevorgian, and R. Wallen, "Sequence impedance measurement of utility-scale wind turbines and inverters – reference frame, frequency coupling, and MIMO/SISO forms," *IEEE Trans. Energy Conv.*, vol. 37, no. 1, pp. 75-86, Mar. 2022.